Multi-trajectory Pose Correspondences using Scale-dependent Topological Analysis of Pose-Graphs

Sayantan Datta
sayantan.datta@research.iiit.ac.in

Avinash Sharma
asharma@iiit.ac.in

K Madhava Krishna
mkrishna@iiit.ac.in

***Abstract*— This paper considers the problem of finding pose matches between trajectories of multiple robots in their respective coordinate frames or equivalent matches between trajectories obtained during different sessions. Pose correspondences between trajectories are mediated by common landmarks represented in a topological map lacking distinct metric coordinates. Despite such lack of explicit metric level associations, we mine preliminary pose level correspondences between trajectories through a novel multi-scale heat-kernel descriptor and correspondence graph framework. These serve as an improved initialization for ICP (Iterative Closest Point) to yield dense pose correspondences. We perform extensive analysis of the proposed method under varying levels of pose and landmark noise and showcase its superiority in obtaining pose matches in comparison with standard ICP like methods. To the best of our knowledge, this is the first work of the kind that brings in elements from spectral graph theory to solve the problem of pose correspondences in a multi-robotic setting and differentiates itself from other works.**

I. Introduction

This paper proposes a novel variant of the multi-robot trajectory mapping methods found in the literature [6, 1]. Unlike most previous methods that exchange laser scans or map locations [18, 1, 6] to draw metric associations between poses thereby fusing maps or trajectories, the current method relies on exploiting the topology of the underlying pose-graph to obtain dense pose correspondences across multiple trajectories of one or more robots. Here each trajectory is assumed to be represented in its own coordinate frame. As a consequence, the entailment of the landmark locations in a Cartesian space or range scans with depth information is bypassed.

The motivation for this paper is argued from a situational example, where the autonomous robots or vehicles move through a network of roads, registering their trajectory in their respective reference frames. During the course of their trajectories, they occasionally pass through the same area of the environment. If the information common to them is only a set of images seen by them and represented as landmarks(like road signs or stationary objects), the paper strives to answer the following questions:

1) Given trajectories of two or more robots with a common topological map of landmarks, is it possible to extract those parts of the trajectories (of the respective robots) that have spanned or covered the same area ?
2) Is it possible to obtain metric level correspondences between poses of the trajectories in those common areas covered by them ?

All authors are associated with the Robotics Research Center, IIIT Hyderabad

A. Challenges

Finding dense metric level pose correspondences across overlapping trajectories have following challenges.

- The Cartesian coordinates for landmarks might not be available (e.g. if front end is only using monocular camera) or can have significant noise (e.g. GPS readings can be really noisy).
- There could be significant pose-noise in each trajectories. As a consequence, traditional point-cloud registration methods are not directly suitable.
- There would be significant topological differences in the pose-graphs constructed from trajectories that are only partially overlapping.
- A significant number of landmarks are observed from non-contiguous sections of the trajectory. The dense pose level correspondences solution should respect these constraints.
- Some parts of the trajectories might have many input landmark associations as opposed to some other parts where associations are sparser, as landmarks can not be assumed to be uniformally distributed over the robot trajectories.
- The initial landmark associations across two trajectories might also be noisy (e.g., due to perceptual aliasing).
- Common landmarks which are observed from disparate portions of the trajectory should not affect the performance of the algorithm in terms of inter-trajectory correspondence.

The solution to the above challenges lies in invoking frameworks that exploit the topological properties of the landmark-pose graph. The multi-scale Heat-kernel framework is popularly used for scale-dependent topological characterization of graphs [22]. In Pose-Graphs, this is achieved by formulating some key graph nodes (i.e., selected landmarks) as the heat sources and characterizing all other graph nodes based up on the amount of heat that reaches to them if heat diffusion is performed at multiple scales. Such intrinsic topological characterization is analogous to barycentric coordinate system and yield a dense heat-kernel descriptor for each of the graph nodes. Heat diffusion does not have a direct physical interpretation in our case and it merely acts as an intrinsic metric over the pose-graph. The multi-scale characterization is advantageous over the single scale as it enables dealing with non-uniform distribution of heat sources (landmark nodes) over the graph. Additionally, it allows simultaneously characterizing both denser as well as sparser neighborhoods in the graph.

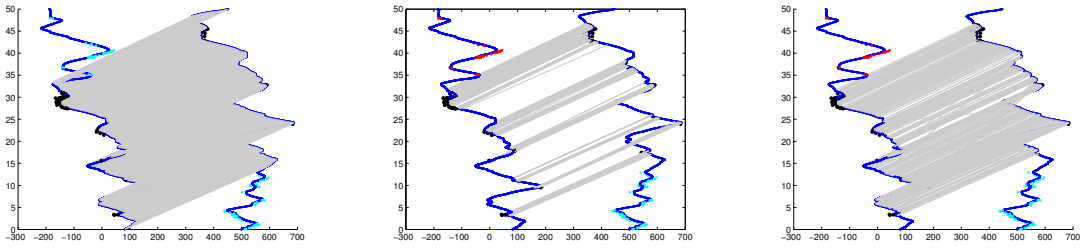

(a) (b) (c)

Fig. 1: The blue lines showcase the trajectory path, and the black dots showcase the landmarks; (a) The trajectory has been split into two, with the ground truth correspondences(gray lines) among them; (b) The output of Correspondence Graph solution using multi-scale heat-kernel pose descriptors; (c) Dense binary correspondence established by ICP initialized with output correspondences shown in (b).

Such multi-scale topological characterization of pose-graphs addresses the previously listed challenges in following manner. *First,* a purely topological approach that manages to find pose correspondences can bypass the need of metric coordinates for landmarks. *Second*, since between pose relations over the same trajectory can be modeled as a topological relation with constant edge weights the problem of pose noise stands circumvented. *Third*, the non-overlapping part of the trajectories can be handled by only focusing on local neighborhoods in each of the trajectory where landmark associations are known in advance. This can be achieved by a scale dependent characterization of pose-graphs which can address the challenge of topological noise. *Fourth,* the heat diffusion based topological characterization would inherently exploit the explicit or indirect loop closure constraints and ensure that final output correspondence respect them. *Fifth,* the challenge of non-uniformity in distribution of landmarks over trajectories can be addressed by exploiting the multi-scale behavior. A small scale neighborhood characterization is helpful in the parts of trajectories with large number of landmarks as oppose to the areas with much sparser landmarks where a large scale characterization is needed. *Finally,* the issue of landmark association noise can be handled by selecting more than one landmark as heat sources while characterizing neighboring poses. We show performance of proposed method on both real as well as synthetic data and show robust performance with varying parameters and noise.

B. Our Contribution

1) Proposed a novel multi-scale heat-kernel descriptor capable of finding poses proximal to each other between trajectories (each trajectory represented in its own local coordinate frame), capitalizing on the inherent topological similarities between the respective pose-graphs at varying scales. Subsequently these matching poses are robustified using a correspondence graph by solving for its approximate maximal clique using the spectral relaxation algorithm as proposed in [17].
2) The proposed method achieves higher precision inter-pose associations than ICP based/inspired methods. This is achieved despite ICP based methods being initialized with metric correspondences of landmark poses unavailable to the current method. This is based on the observation that ICP, being an EM algorithm, demonstrates improved convergence behavior with good initialization.

Though a multi-trajectory pose-graph optimization can be formulated using these dense pose level correspondences, this paper is more concerned with improving the precision of the pose level correspondences. Figure 1 shows the expected (ground truth), intermediate (preliminary pose level correspondences) and final dense correspondence output of the proposed method on two trajectories obtained from Victoria Park dataset(VP) [21].

II. Related Work

Cooperative concurrent mapping and localization proposed in [10], merges the sensor and navigation information from multiple autonomous vehicles. Manifold representation and patch based technique was proposed .in [14]. Particle filter approaches to the problem have been explored in [15]. An approach using square root information smoothing was presented Anderson's work [1]. A related work on localizing using road maps and visual odometry was also investigated in [5].

Prior contributions without assuming initial poses between robots have been made in [7] followed by [8]; which use a triangulation-based robust estimator for matching feature maps eventually using a RANSAC based approach for Robot data association and initialization of relative frames of reference, to align individual maps. [19] invokes RANSAC algorithm for implementing a distributed scheme for robust data fusion.

The transfer overhead reduction was attempted in [16], using condensed measurement. However, such methods are susceptible to noise over several pose scans. A common trend of using laser scans as map information has also been prevalent in [1]. [18] creates pose matches across multiple slam sessions by matching 2D laser scans. Nonetheless, the laser based systems can be unavailable due to cost and other factors.

Heat-kernel framework [2] is an important and popular multi-scale graph analytics paradigm and has been successfully employed for solving various computer vision applications [22, 20]. Our recent work used this framework for

filtering significant outliers loop closure edges in the pose-graphs [9].

III. Background

In this section we will introduce two important mathematical building blocks of our proposed approach.

A. Heat-Kernel Framework

The spectral graph theory enables Euclidean embedding of the graph using the spectrum of graph Laplacian matrix. In this space, Euclidean distance between graph node approximate average connectivity over the graph. [9]

Let $G = \{V, E, W\}$ be an undirected weighted graph where $V = \{v_1, \cdots, v_n\}$ be the set of graph nodes represented by (not-necessarily) some Euclidean coordinates, $E = \{e_1, \cdots, e_m\}$ be the set of undirected edges and W be the $n \times n$ square symmetric weighted adjacency matrix of the graph with each entry $\mathbf{W}_{ij} \geq 0, \ \forall\, i, j \in \{1, \cdots, n\}$.

The graph Laplacian matrix $\boldsymbol{L}$ can be derived as:

$$\boldsymbol{L} = \mathbf{D} - \mathbf{W}, \tag{1}$$

where $\mathbf{D}$ is the diagonal degree matrix of the graph with each non-zero diagonal entry $d_i = \sum_{j=1}^{n} \mathbf{W}_{ij}$.

Let

$$\boldsymbol{L} = \mathbf{U}\Lambda\mathbf{U}^T \tag{2}$$

be the eigen-decomposition of the $\boldsymbol{L}$ matrix where $\mathbf{U} = [\vec{u}_1, \cdots, \vec{u}_n]$ be the eigen vectors and $\Lambda = Diag(\lambda_1, \cdots, \lambda_n)$ be the corresponding eigenvalues of the $\boldsymbol{L}$ matrix with property that $\{0 = \lambda_1 \leq \lambda_2 \leq \cdots \leq \lambda_n\}$ and $\vec{u}_1 = \vec{1}$ for a connected graph.

Heat diffusion on graphs is exactly the parallel of diffusion on closed Riemannian manifolds where the heat-kernel matrix is defined as [2]:

$$\mathbf{H}(t) = e^{-\boldsymbol{L}t}. \tag{3}$$

We consider real-valued functions $\vec{f}$ over V, $\vec{f}$: $V \to \mathbb{R}$ and we note that $\vec{f} = (f_1, \cdots, f_n)^T$ is simply a vector indexed by the nodes of G. The vector $\vec{f}(t) = \mathbf{H}(t)\vec{f}$ is a solution to the heat-diffusion equation $(\frac{\partial}{\partial t} + L)\vec{f}(t) = 0$.

Hence, $\vec{f}$ corresponds to some initial heat distribution over the nodes of graph G, and $\vec{f}(t)$ is the heat distribution at time/scale t starting from $\vec{f}(0) = \vec{f}$. Starting with a point heat distribution, at node v_j, $\vec{f}_j(0) = [0, \cdots, 1, \cdots, 0]^T$, the heat distribution at time t is given by the jth column of the heat matrix which is denoted by $\mathbf{H}(:, j; t)$ as

$$\vec{f}_j(t) = \mathbf{H}(t)\vec{f}_j(0) = \mathbf{H}(:, j; t) \tag{4}$$

From Eq. 4 we can obtain a straightforward interpretation of the entries of the heat matrix, namely each entry $h(i, j; t)$ of H(t) corresponds to the amount of heat available at node v_i at time t, starting with a point heat distribution at node v_j. The symmetric function h: $V \times V \to \mathbb{R}$ is the heat-kernel of a graph G. Each diagonal term $h(i, i; t)$ of the heat-kernel matrix has an interesting interpretation as well. It corresponds to the amount of heat remaining at node v_i at time t. To conclude, the heat-kernel matrix encapsulates important intrinsic information about how heat travels from one part of the graph to another part or in a way heat diffusion at different scales can be used to capture scale-dependent topological characterization of graphs.

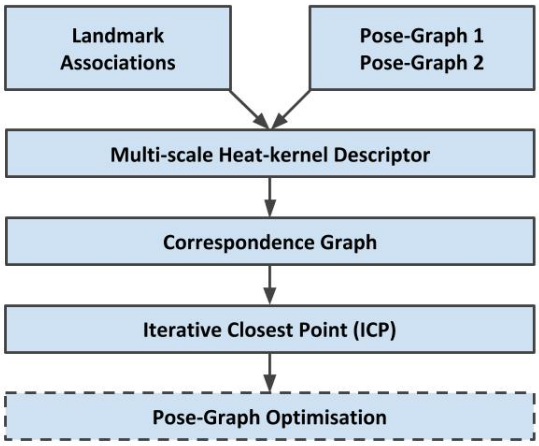

Fig. 2: Overview of the proposed method.

B. Correspondence Graph Framework

Correspondence graphs have been used in robotics [3] to model the problem of data association. The idea is to model each potential match across two feature sets as a node whereas an edge capture mutual consistency among them. The most consistent set of correspondences are given by the maximal weighted clique of this graph.We adapt a spectral relaxation solution [17] for maximal clique detection. In this solution, the elements of eigenvector (associated with largest eigenvalue) of the correspondence graph adjacency matrix are sorted in the decreasing order. The correspondence associated with largest element is accepted while other conflicting ones are dropped from the selection list. Similarly, next best correspondence is found until all one to one feature level correspondences are established.

IV. Proposed Method

A. Overview

Figure 2 depicts the building blocks and overall pipeline of the proposed approach. Each of these blocks are discussed in detail below.

Mathematical Notations

Let the two pose-graphs be represented as $G^1 = \{(V^1 \cup L^c), E^1, \mathbf{W}^1\}$ and $G^2 = \{(V^2 \cup L^c), E^2, \mathbf{W}^2\}$. Here, V^k, E^k are the sets of poses and undirected edges for each graph G^k where $\mathbf{W}^k$ is the associate weighted adjacency matrix. Let L^k is the sets of landmarks associated to each graph G^k then L^c be the set of common (and may be noisy) landmarks such that $L^c = L^1 \cap L^2 = \{l_1, \cdots, l_Q\}$. It is important to note that $l_i \in L^c$ represents the landmark but do not expect it's Cartesian coordinates to be known. Each element $\omega_{ij}^k \geq 0$ of $\mathbf{W}^k$ is defined as the weight for either an odometry edge, or an edge connecting pose and landmark node. As $\mathbf{W}^k$ is a squared symmetric matrix, $\omega_{ij}^k = \omega_{ji}^k$. We consider $\omega_{ij}^k = 0.7, \forall (i \in V_i^k, j \in L_j^k)$ pairs and $\omega_{ij}^k = 0.9, \forall (i \in V_i^k, j \in V_j^k)$ pairs. We have intentionally

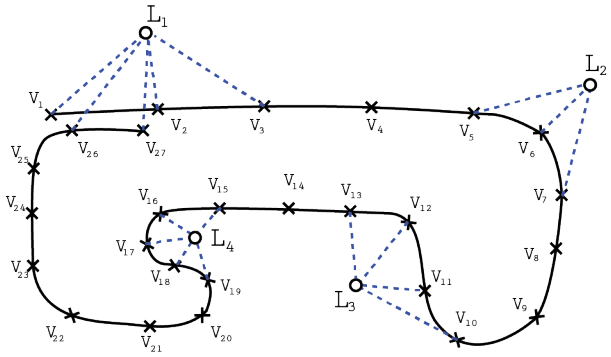

Fig. 3: A basic trajectory with 27 poses (marked as 'x') and 4 landmarks (marked as 'o'). The solid lines represent odometry while the dashed line represents landmark-pose edges.

put relatively higher weighing for odometry edges than for landmark-pose edges, so that we can insist on having more reliability on odometric observations as compare to pose-landmark association coming from the front end.

B. Heat-Kernel Descriptor

The graph Laplacian matrix for each input pose-graphs can be computed using the weighted adjacency (see Eq. 1).The heat-kernel matrices $\mathbf{H}^k(t_p)$ is subsequently calculated for $k = 1, 2$ and $\forall t_p \in T = \{t_1, \cdots, t_P\}$ using Eq.3. As explained in section III, each element $h^k_{i,j}(t_p)$ of the symmetric $\mathbf{H}^k(t_p)$ matrix stores the amount of heat transferred from landmark node l_j (considering it as a unit heat source) to the pose node v_i while diffusing heat at scale t_p.

The heat descriptor $\mathbf{R}^k_{v_i}$ for node i in graph G^k is computed by constructing a $P \times Q$ matrix. Where P is the number of time scale parameters (varying from a small scale to large scale values i.e., $t_1 \mapsto 0$ and $t_P \mapsto \infty$) used for heat diffusion (see implementation details in section V), and $Q = len(L^c)$ is the number of common landmarks between the two trajectories for which initial association is assumed to be given.

We can see in a toy example depicted graphically in Figure 3, let $Q = 4$ be the number of common landmarks. Now if we diffuse heat at 3 different scales (i.e., $t_p \in \{t_1, t_2, t_3\}$), our heat-kernel descriptor matrix for node $v^k_i \in V^k$ would be a 4×3 size matrix, where each element in the row would be the amount of heat reached from $l^k_j \in L^c$ to v^k_i at 3 different scales of heat diffusion. In general, we can define the heat-kernel descriptor for node v_i in pose-graph G^k as a matrix of size $Q \times P$:

$$\mathbf{R}^k_{v_i} = \begin{bmatrix} h^k_{i1}(t_1) & \cdots & h^k_{i1}(t_P) \\ \vdots & \vdots & \vdots \\ h^k_{iQ}(t_1) & \cdots & h^k_{iQ}(t_P) \end{bmatrix} \tag{5}$$

Descriptor Matching

Given any two heat-kernel descriptors $\mathbf{R}^1_{v_i}$ and $\mathbf{R}^2_{v'_i}$ from pose-graph G^1 and G^2, we propose to use the weighted Euclidean distance to compute a matching score between two descriptors as:

$$score(i, i') = \sqrt{tr(((\mathbf{R}^1_{v_i} - \mathbf{R}^2_{v'_i})\Psi^{1/2})^T((\mathbf{R}^1_{v_i} - \mathbf{R}^2_{v'_i})\Psi^{1/2}))} \tag{6}$$

A lower score signifies a better match and vice-versa. The dimension weighting matrix is defined as $\Psi = diag[\psi_1, \cdots, \psi_P]$ where $0 \leq \psi_i \leq 1$ is the weight given to scale t_i. The Ψ matrix addresses the challenge posed by the non-uniform distribution of landmarks across the trajectory. As nodes in the vicinity of several landmarks have a significantly higher informative heat-kernel descriptor than nodes having very less number of landmarks in their neighborhood, we exploit multi-scale behavior of heat-kernel descriptors by setting the weights in such a way that for nodes with neighborhood of numerous landmarks, we give more importance to the descriptors entries (dimensions) that are associated with small scale heat-diffusion. Similarly, for nodes with neighborhood of fewer landmarks, we give more importance to the descriptors entries (dimensions) that are associated with large scale heat-diffusion.

C. Correspondence Graph

To improve on the global consistency of the matches introduced by the heat-kernel descriptors, we have exploited the technique of correspondence graphs. (see section III for details).

Given two sets of descriptors from pose-graphs (G^1 and G^2), we construct a correspondence graph $\mathtt{G_{cors}}$ with following details. For every pair of nodes $(i, i') : i \in V^1, i' \in V^2$ there is an associated score that measures how well $R^1_{v_i} \in G^1$ matches $R^2_{v'_i} \in G^2$. We consider matching only the descriptors from two pose-graphs for which respective nodes belong to the neighborhood of the common landmarks. If these descriptors match with a score below the threshold value θ, we consider them as a potential candidate assignment. Let n be the number of such assignments. Each of them can be modeled as a node of the correspondence graph.

We model our pairwise affinity among candidate assignments $a = (i, i')$ and $b = (j, j')$ by comparing the number of odometry steps between nodes (i, j) over G^1 and similarly between (i', j') over G^2, respectively. A lower difference in the number of steps invokes a higher affinity and vice versa. We implemented an inverse exponential kernel over the differences in odometry steps, to get the required affinity. Let M be the $n \times n$ weighted affinity matrix of the correspondence graph where each symmetric entry is the value of pairwise affinity among two candidate assignments.

The list of solution correspondences from binary vector x is explicitly stored as node index pairs in $C = \{c_k, c_m\}$ where $c_k = (i, i')$.

We find out an approximation of the largest clique in the correspondence graph and obtain the binary correspondences by adopting the algorithm which is well explained in [17].

D. Iterative Closest Point

The above obtained correspondences feed into the well known ICP algorithm as supervised initializations. ICP as we know is an algorithm employed to calculate a rigid transformation that registers a point cloud to another, thereby

minimize the difference between two clouds of points. For our case, we have used point to point minimization metric, as described in [4]

V. Experiments and Results

We have conducted extensive experiments on various standard datasets and evaluated our method using the standard metric of mean Precision and mean Absolute Trajectory Error (ATE). We pose the trajectory merging problem as point-cloud registration. Therefore performance of the proposed framework has been compared against ICP like method which are de-facto standards for point cloud registrations.

For the purpose of benchmarking our results, we propose a supervised ICP algorithm (sICP) that is initialized with landmark associations between trajectories. Here we assume that landmark coordinates are known to enable the initialization. As we show subsequently that our method despite lacking such metric level initializations is still able to outperform sICP.

Supervised Iterative Closest Point (sICP)
It is a variation of the previously mentioned ICP algorithm. The standard ICP is supervised in two steps, *Firstly*, we find an initial transformation $R|T$ of G^1 by applying ICP on the initial association of landmarks coordinates among G^1 and G^2. This $R|T$ is applied on the v_i^1. This serves as an initialization for the ICP to be applied on the graph poses. *Secondly,* we crop the number of poses, both on G^1 and G^2, on which to apply ICP on by removing the graph poses which are topologically distant from the associated landmarks. This reduces point to point matching anomalies induced by extraneous non-overlapping information.

A. Data and Model Experiments

Datasets
We are using two standard real datasets, namely, Victoria Park [21] (VP) and Kitti00 [13]. We split trajectories in various parts to simulate a multi-robot trajectory session. We consider both pose noise and landmark coordinate noise.

Pose-Noise Model: Pose Noise can be modeled as a successive noise model which adds a δ times average odometry length μ_{odom}, to every pose in a cumulative manner. The new pose coordinates are computed as:

$$v_i^k = \mathbb{Q}_{i,(i-1)}^k * v_{i-1}^k + \delta N(0, \sigma_{odom})\mu_{odom} \tag{7}$$

where v_i^k is the i-th pose-node of k-th pose-graph, $\mathbb{Q}_{i,(i-1)}^k$ is the original odometric transformation between the two poses. An example set of trajectories with and without pose noise has been shown in Figure 4.

Landmark Coordinate Noise: The Landmark Coordinate Noise model adds a γ times the mean sequentially pairwise landmark distance ($\mu_{landmark}$), to every landmark independently. The new landmark coordinates are computed as:

$$l_i^k = l_i^k + \gamma N(0, \sigma_{landmark})\mu_{landmark} \tag{8}$$

where l_i^k is the i-th landmark-node of k-th pose-graph.

Experiment on Real Data
Our proposed algorithm has been tried out in an outdoor multi-session dataset, where a Husky™ Robot fitted with a Bumblebee™ stereo camera have been used to take two individual datasets of around 100 metres each. The datasets are consecutive such that each of the robot overlaps a portion of the other's trajectory.

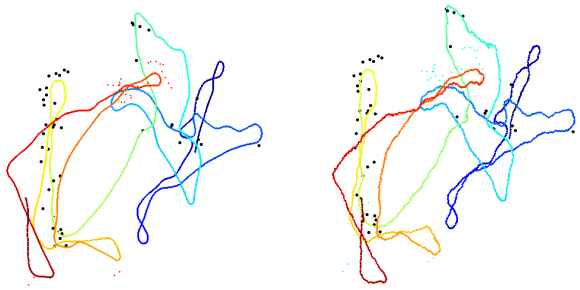

(a) (b)

Fig. 4: The colored path shows the trajectory of the robot. The dots show the landmarks. (a) Shows a trajectory without pose noise, while (b) is the trajectory with added successive pose noise.

B. Choice of Parameters

The time scale parameter vector T^k, which is useful for computing the heat-kernel descriptors for trajectory pose-graph G^k, is obtained by using the inverse logarithmic map of $d = e^{(-\lambda_j^k . t)}$ for specific values of λ_j^k and d. Here, λ_j is the jth eigenvalue of the associated graph Laplacian matrix where the value of jth index is typically set to be the 5% of total number of nodes in the respecting trajectory. This enables normalization of scale parameter in case of trajectories with significantly different n and topological variations. For a fixed j, the different values of d parameters yield respective scale parameters that are used as elements of T^k vector. E.g., we have used values of d as $[0.99, 0.95, 0.90, 0.85, 0.80, 0.75]$ which yields the scales as

$$T^1 = [0.30, 1.55, 3.18, 4.90, 6.73, 8.67]$$

$$T^2 = [0.04, 0.23, 0.49, 0.75, 1.04, 1.34]$$

for trajectory shown in Figure 4. For kitti00, the same values for d, generates

$$T^1 = 0.1808, 0.9229, 1.8957, 2.9241, 4.0149, 5.1762]$$

$$T^2 = [0.1159, 0.5916, 1.2151, 1.8744, 2.5735, 3.3179]$$

It is important to note that, T^1 and T^2 vectors for two pose-graphs G^1 and G^2 can be different depending on the variation in the respective graph topologies.

C. Evaluation Metrics

To determine the performance of our algorithm, we compute both the precision as well as the translation error inflicted by the incorrect correspondences. For the former, we calculate the true positive rate of the correspondences established by our algorithm. For the latter, we select the Absolute Translation Error(ATE) error. It is important to note that for computing ATE, we project our matches to ground truth trajectory (computable from optimization of single original trajectory), and then calculate the mean squared error over it.

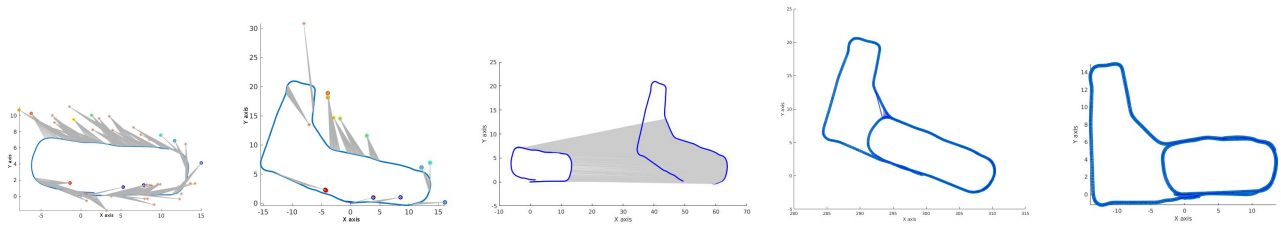

(a) (b) (c) (d) (e)

Fig. 5: **(a),(b)**: shows the independent g2o trajectories. The landmark-pose associations are marked with gray. (c) shows the dense pose association (gray) among the poses in the two trajectories. (d) showcases the optimized trajectory with the our computed dense correspondence, (e) shows the optimized trajectory computed from associations created using front-end libViso and DLoopDetector [11].

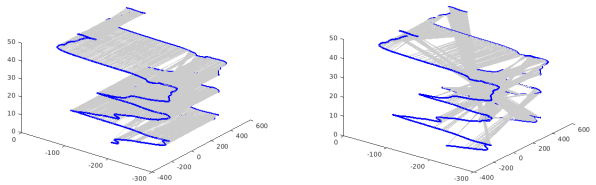

(a) (b)

Fig. 6: (a) Shows results of our algorithm (our initialization + ICP), while (b) shows results of supervised ICP, (landmark initialized + ICP); for the VP dataset. Just the cropped section of the trajectory is shown on the optimized section, for visualization purposes.

TABLE I: Performance over Varying Pose-noise

Dataset	Pose Noise δ	ATE		Precision	
		ours	sICP	ours	sICP
Victoria Park	1	1.43	66.84	0.91	0.31
	3	3.42	52.58	0.66	0.30
	5	5.91	53.23	0.47	0.16
Kitti00	1	1.04	100.56	0.94	0.25
	3	1.86	138.60	0.76	0.12
	5	4.04	125.90	0.42	0.07

In order to compute precision, we have compared the pose correspondences to that of the ground truth associations of poses. Since we are allowing significant (accumulative) pose-noise model, we relax the definition of precision by accepting a drift in matching inside a neighborhood of approximately 0.1% of the average number of pose nodes in the respective pose-graphs.

D. Results

Qualitative Comparison

Here we show qualitative results on VP dataset where we have added a pose-noise with $\delta = 4$ and $\gamma = 7$. Figure 6 shows the comparison between the output of the proposed method v/s a supervised ICP algorithm. Although, both figures show dense binary correspondences obtained from ICP algorithm, we can see that the output of ICP initialized with only landmark associations (with Cartesian coordinates) are inferior as compared to results obtained with proposed method (which do not consider landmark Cartesian coordinates) on the same set of trajectories with same input landmark associations.

Pose-noise Variations

We have used both VP and Kitti00 dataset for comparing robustness of our method and benchmark sICP in the presence of varying pose-noise in each of the pose-graph. We have evaluated the performance of the two algorithms using ATE and precision while varying the pose-noise for δ being $1, 3$ *and* 5 (see Eq. 7 for details). This cumulative Gaussian noise was added in 6 independent experiments and the mean ATE and precision values are reported in the Table I for both the datasets.

Landmark Coordinate-noise Variations

We have corrupted the ground truth landmark coordinates for both VP and Kitti00 datasets by setting five different values of $\gamma = \{2, 5, 7, 10, 12\}$ in Eq. 8. This independent Gaussian noise to landmark coordinates was added in for three values of $\delta = \{1, 3, 5\}$ and the mean ATE and precision values are reported in the Table II.

We see that our proposed method provides consistently better results than sICP even for higher landmark coordinate-noise levels. Please note that the mean ATE for sICP can drop significantly low (and the respective mean precision for sICP can go high) for close to zero pose-noise. However, majority of the real-world scenarios this will not be the case and hence our method which is utterly invariant to landmark-coordinate noise should be preferred of sICP.

We see that our proposed method provides consistently better results than sICP even for higher pose-noise levels. It is important to note that the pose-noise is significant high, as it is a cumulative noise and hence the overall pose-noise can increase dramatically (e.g., in case of VP where approximately 5000 poses are there on each trajectory).

Experiment on Real World

The odometry of the land robot has been calculated using libViso2 [12]. libViso2 was also used to reconstruct the landmark points. Provided with 11 non metric landmark associations among the two trajectories, our attempt to mine pose relations have been showcased in Figure 5. Here, we find that even when the trajectory is not exactly overlapping, we are still able to come up with reasonable correspondences.

g2o Optimization over merged Trajectories

As a consequence of obtaining dense pose correspondences, we are able to merge trajectories as well. Figure 7 shows two optimized trajectories on the VP Dataset. On the left (a) is the g2o optimized trajectory computed using the original single trajectory (can be treated as ground truth here). On the right side (b) is the g2o optimized trajectory obtained by merging the two overlapping and independently

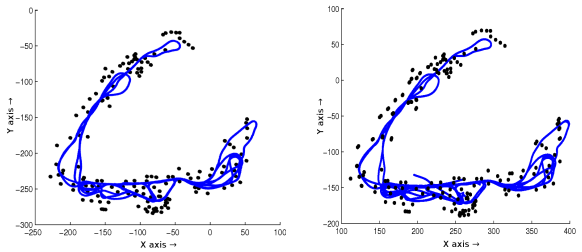

(a) (b)

Fig. 7: (a) The g2o optimized trajectory obtained by original single trajectory. (b) The g2o optimized trajectory obtained by exploiting pose level correspondences between the split trajectories.

TABLE II: Performance over Varying Landmark Coordinate-noise

Dataset	Landmark Coord. Noise	ATE		Precision	
		ours	sICP	ours	sICP
Victoria Park	2	3.74	3.74	0.57	0.68
	5	3.74	5.04	0.57	0.50
	7	3.74	35.45	0.57	0.53
	10	3.74	42.71	0.57	0.44
	12	3.74	78.67	0.57	0.02
Kitti00	2	2.22	2.24	0.73	0.72
	5	2.22	120.03	0.73	0.09
	7	2.22	2.24	0.73	0.72
	10	2.22	31.5	0.73	0.49
	12	2.22	121.69	0.73	0.15

corrupted trajectories, as discussed above. In this care the split overlapping trajectories were corrupted with following noise parameters: ($\delta = 4$ and $\gamma = 7$).

Figure 5 shows trajectories taken in the campus. They are independent trajectories, with inexact overlap between them. We mine dense correspondences between the parts of the two trajectories that are proximal to one another. Further we successfully merge the trajectories into a single unified frame, through a backend g2o optimization. Moreover, these results obtained are comparable to the results of trajectory merging obtained through point cloud correspondences of the common landmarks shown in Figure 5(e)

E. Discussion

Considering our proposed method only takes into account the graph structures of the individual trajectories, one drawback is that trajectory correspondences of non proximal overlap are only obtained to be qualitatively accurate. The method is also susceptible to large noise in the initial landmark associations and are susceptible to symmetrical neighborhood in the pose-graph. However, these are classical limitations for almost all existing methods.

The main theme and contribution of the paper is not its performance vis-à-vis ICP like approaches, but rather in its ability to mine metric level inter pose correspondences given what was merely a set of topological relations lacking a distinct metric character. To the best of our knowledge, such a topological pose-graph analysis approach for multi-trajectory alignment problem was not proposed in robotic literature earlier.

VI. Conclusion and Future Work

We have proposed a novel heat-kernel descriptor and correspondence graph modeling for obtaining dense pose level correspondences across multiple unoptimized trajectories. The key achievement of the proposed method is to find dense pose level correspondences using only the topological landmark association. We have provided extensive results under varying levels of pose and landmark coordinate-noise and showcase its superiority in obtaining associations in comparison with ICP like methods.

As part of the future work, we would like to formulate a more sophisticated multi-trajectory optmization framework that can better exploit the dense pose level correspondences across trajectories.

VII. Acknowledgment

This work was supported by the Centre for Artificial Intelligence and Robotics, Defence Research and Development Organization, Government of India.

References

[1] Lars AA Andersson and Jonas Nygards. “C-SAM: Multi-robot SLAM using square root information smoothing”. In: *ICRA*. 2008, pp. 2798–2805.

[2] Xiao Bai and Edwin R Hancock. “Heat kernels, manifolds and graph embedding”. In: *Structural, Syntactic, and Statistical Pattern Recognition*. 2004, pp. 198–206.

[3] Tim Bailey et al. “Data association for mobile robot navigation: A graph theoretic approach”. In: *ICRA*. Vol. 3. 2000, pp. 2512–2517.

[4] Paul J Besl and Neil D McKay. “Method for registration of 3-D shapes”. In: *Robotics-DL tentative*. 1992, pp. 586–606.

[5] Marcus A Brubaker, Andreas Geiger, and Raquel Urtasun. “Lost! leveraging the crowd for probabilistic visual self-localization”. In: *CVPR*. 2013, pp. 3057–3064.

[6] Alexander Cunningham, Vadim Indelman, and Frank Dellaert. “DDF-SAM 2.0: Consistent distributed smoothing and mapping”. In: *ICRA*. 2013, pp. 5220–5227.

[7] Alexander Cunningham, Manohar Paluri, and Frank Dellaert. “DDF-SAM: Fully distributed SLAM using constrained factor graphs”. In: *IROS*. 2010, pp. 3025–3030.

[8] Alexander Cunningham et al. “Fully distributed scalable smoothing and mapping with robust multi-robot data association”. In: *ICRA*. 2012, pp. 1093–1100.

[9] Sayantan Datta et al. “SLAM pose-graph robustification via multi-scale Heat-Kernel analysis”. In: *Decision and Control (CDC), 2016 IEEE 55th Conference on*. IEEE. 2016, pp. 2912–2919.

[10] John W Fenwick, Paul M Newman, and John J Leonard. “Cooperative concurrent mapping and localization”. In: *ICRA*. Vol. 2. 2002, pp. 1810–1817.

[11] Dorian Gálvez-López and J. D. Tardós. “Bags of Binary Words for Fast Place Recognition in Image Sequences”. In: *IEEE Transactions on Robotics* 28.5 (2012), pp. 1188–1197.

[12] Andreas Geiger, Julius Ziegler, and Christoph Stiller. “StereoScan: Dense 3D Reconstruction in Real-time”. In: *IV*. 2011.

[13] Andreas Geiger et al. “Vision meets robotics: The KITTI dataset”. In: *IJRR* (2013).

[14] Andrew Howard. “Multi-robot mapping using manifold representations”. In: *ICRA*. Vol. 4. 2004, pp. 4198–4203.

[15] Andrew Howard. “Multi-robot simultaneous localization and mapping using particle filters”. In: *IJRR* 25.12 (2006), pp. 1243–1256.

[16] Maria Teresa Lazaro et al. “Multi-robot SLAM using condensed measurements”. In: *IROS*. 2013, pp. 1069–1076.

[17] Marius Leordeanu and Martial Hebert. “A spectral technique for correspondence problems using pairwise constraints”. In: *ICCV*. Vol. 2. 2005, pp. 1482–1489.

[18] John McDonald et al. “6-DOF multi-session visual SLAM using anchor nodes”. In: (2011).

[19] Eduardo Montijano, Sonia Martinez, and Carlos Sagues. “Distributed robust data fusion based on dynamic voting”. In: *ICRA*. 2011, pp. 5893–5898.

[20] Venkatesh Murthy et al. “Image Annotation using Multi-scale Hypergraph Heat Diffusion Framework”. In: *ICMR*. 2016.

[21] Eduardo Nebot. *The Sydney Victoria Park dataset*. 2009.

[22] Avinash Sharma et al. “Topologically-robust 3D shape matching based on diffusion geometry and seed growing”. In: *CVPR*. 2011, pp. 2481–2488.